Composite steel beam database for seismic design and performance assessment of composite-steel moment-resisting frame systems

Hammad El Jisr · Ahmed Elkady · Dimitrios G. Lignos

Abstract This paper discusses the development of a publicly available database of composite steel beam-to-column connections under cyclic loading. The database is utilized to develop recommendations for the seismic design and nonlinear performance assessment of steel and composite-steel moment-resisting frames (MRFs). In particular, the sagging/hogging plastic flexural resistance as well as the effective slab width are assessed through a comparison of the European, American and Japanese design provisions. The database is also used to quantify the plastic rotation capacity of composite steel beams under sagging/hogging bending. It is found that the Eurocode 8-Part 3 provisions overestimate the plastic rotation capacities of composite beams by 50% regardless of their web slenderness ratio. Empirical relationships are developed to predict the plastic rotation capacity of composite steel beams as a function of their geometric and material properties. These relationships can facilitate the seismic performance assessment of new and existing steel and composite-steel MRFs through nonlinear static analysis. The collected data underscores that the beam-to-column web panel zone in composite steel beam-to-column connections experience higher shear demands than their non-composite counterparts. A relative panel zone-to-beam resistance ratio is proposed that allows for controlled panel zone inelastic deformation of up to 10 times the panel zone's shear yield distortion angle. Notably, when this criterion was imposed, there was no fracture in all the examined beam-to-column connections.

Keywords Composite steel beam database · seismic performance assessment · composite floors · Plastic rotation capacity · Panel zone shear resistance

H. El Jisr . A. Elkady . D. G. Lignos (✉)
School of Architecture Civil and Environmental Engineering, École Polytechnique Fédérale de Lausanne, Lausanne, Switzerland
e-mail: dimitrios.lignos@epfl.ch
tel: +41 21 69 32427

1. Introduction

Modern seismic design provisions adopt capacity design principles that allow for controlled inelastic deformations within a lateral-load resisting system (Fardis 2018). In the case of steel and composite-steel moment-resisting frame (MRF) systems, steel beams act as the primary structural fuse to dissipate the seismic energy. Prior studies (Lignos et al. 2013; Elkady and Lignos 2014, 2015) suggest that the amplified flexural resistance of composite steel beams could shift the plastic hinge formation to the MRF columns despite the fact that a strong-column/weak-beam (SCWB) criterion was imposed. Subassembly tests on deep beams (depth, h = 913 mm) with partial composite action (Uang et al. 2000; Jones et al. 2002), showed that their sagging flexural resistance (i.e. slab in compression) amplified by about 10% to 20% relative to the bare beam plastic bending resistance. Similarly, beams with a depth of 753 mm tested by Civjan et al. (2001) developed a sagging flexural resistance amplification of 10% to 30%. Elkady and Lignos (2014) assessed the hysteretic behavior of composite steel beams with reduced beam section (RBS) with depths varying between 533 mm and 911 mm. These sizes are typically used in perimeter steel MRFs in North America. They found that the composite slab amplifies the sagging flexural resistance, on average, by 35%. In Japan and Europe, the use of space steel MRFs is promoted. This typically leads to the selection of shallow beams (h = 300 to 500 mm) even in tall buildings (Nakashima et al. 2000; Mele 2002). The amplification of the sagging flexural resistance in such beams is even more pronounced. In particular, Nakashima et al. (2007) showed that the composite action amplifies the sagging flexural resistance of 400 mm deep beams by up to 50%. This agrees with pior experimental studies (Bursi and Gramola 2000; Bursi et al. 2009).

The potential deficiencies associated with disregarding the composite action in seismic design can be alleviated by (a) totally disconnecting the slab from the column face (Tremblay et al. 1997); (b) by employing a larger SCWB ratio (Elkady and Lignos 2014); or (c) by explicitly considering the expected composite beam flexural resistance in the SCWB check. The European (CEN 2004a), American (AISC 2016a) and Japanese (AIJ 2010a) seismic design provisions compute the flexural resistance of composite steel beams differently. The main two reasons are the variations in the assumed effective width of the slab and the shear strength of the studs. The sensitivity of the flexural resistance of composite steel beams to the above assumptions has not been consistently quantified through direct comparisons with available experimental data.

Nonlinear modeling recommendations (e.g. ASCE/SEI 41-17 and Eurocode 8-Part 3) for the seismic assessment of new and existing structures (ASCE 2017; CEN 2005a) compute a beam's elastic flexural stiffness and plastic rotation capacity by ignoring the composite action. Nam and Kasai (2012) analyzed data from full-scale shake table experiments (Suita et al. 2008; Lignos et al. 2013) and showed that the presence of the slab may increase the beam stiffness by two to three times. Similarly, system-level tests (Nakashima et al. 2007) indicated that the composite steel beam stiffness was twice as high compared to that of a non-composite beam. Prior subassembly tests (Engelhardt et al. 2000; Roeder 2000; Zhang et al. 2004) suggest that, depending on the slab arrangement and the associated degree of composite action, the plastic rotation capacity of a composite steel beam under sagging bending could be up to 80% larger than that of a non-composite beam. In a more recent study, Elkady and Lignos (2014) assessed the plastic rotation capacity of composite deep beams with RBS. Those experienced an 80% and 35% increase in their pre- and post-capping plastic rotations, respectively, compared to non-composite steel beams (capping refers here to the onset of local and/or member geometrical instabilities). However, the above data-set did not cover shallow beams commonly seen in the European and Japanese design practice. This is particularly important for seismic performance assessment methodologies consistent with Eurocode 8-Part 3 (CEN 2005a).

A side issue related to the composite action effect is the increase in the shear demand on the beam-to-column web panel zone (Leon et al. 1998; Elkady and Lignos 2014). This could augment the panel zone inelastic deformations. It is desiriable to allow for controlled panel zone inelastic deformation (Krawinkler 1978; Shin and Engelhardt 2013). While moderate levels of inelastic deformation are usually permitted within the various seismic design provisions in Europe, North America and Asia, there is no consensus on what an acceptable panel zone inelastic deformation range should be.

This paper presents the development of a comprehensive experimental database for composite steel beams that addresses all the aforementioned issues. The database is used to assess several performance parameters that influence the cyclic behavior of composite steel beams in fully restrained beam-to-column connections. These parameters include (i) the flexural resistance, (ii) the effective stiffness, and (iii) the pre- and post-capping plastic rotation capacities. The gathered experimental data is also used to assess the shear resistance of the beam-to-column web panel in composite beam-to-column connections. Three design provisions are considered including the European [Eurocode 3, 4 and 8 (CEN 2004a, b; 2005a, b, c)); the US (ANSI/AISC 360-16 (AISC 2016b) and ANSI/AISC 341-16 (AISC 2016a)]; and the Japanese (AIJ 2010a, b) provisions. The paper proposes a set of seismic design recommendations for composite-steel MRFs that could be adopted in future design provisions. Finally, nonlinear modeling recommendations are also proposed for estimating the flexural

resistance, stiffness and plastic rotation capacity of composite steel beams. These recommendations can facilitate the seismic performance assessment of existing steel frame buildings as well as prospective designs.

2. Description of the Assembled Composite Steel Beam Database

The assembled composite steel beam database comprises 24 experimental programs, which are summarized in Table 1. A total of 97 composite steel beams are gathered including 87 from subassembly tests and 10 from system-level experiments. The beam depths, h, range from 300 to 912 mm; shear span-to-depth ratios, L_o/h (L_o is the distance from the column face to the inflection point) range from 3.4 to 11.6; and web slenderness ratios, c/t_w, range from 36.1 to 53.8. Both partially- and fully-composite steel beam data were gathered. The main types of beam-to-column connections include:

- Bolted extended end-plate connections (BEEP) (see Fig. 1a)
- Welded unreinforced flange welded web connections (WUF-W) (see Fig. 1b)
- Reduced beam section connections (RBS) (see Fig. 1c)
- Through diaphragm connections (TD) (see Fig. 1d)
- Retrofitted connections (bottom flange RBS, top and/or bottom welded or bolted haunches, bottom flange horizontal stiffeners, bottom flange cover plate)
- Reinforced concrete column with steel beams (RCS) and concrete filled steel tube (CFT) steel beam-to-column connections

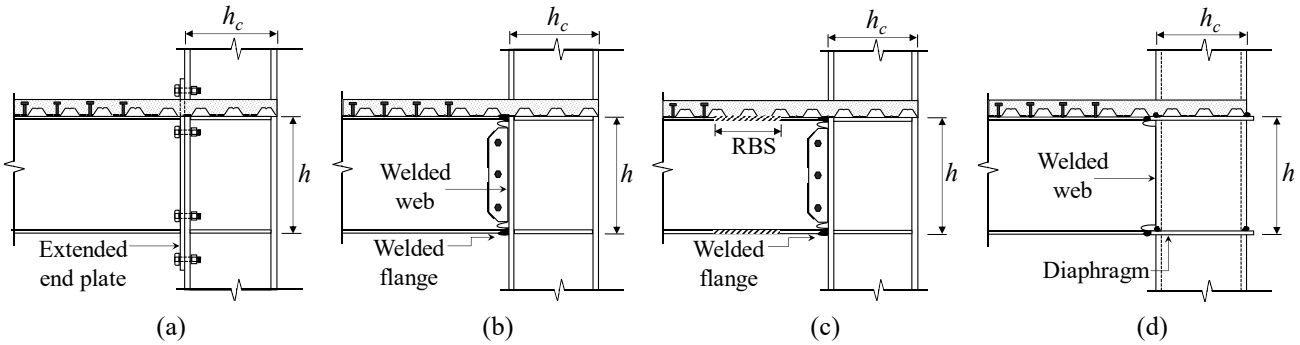

Fig. 1. Typical fully restrained beam-to-column connection types included in the composite steel beam database: (a) BEEP; (b) WUF-W; (c) RBS; (d) TD connection

The collected steel beams are made of 10 steel material types. The measured-to-nominal yield stress ratio ($f_{y,m}$ / $f_{y,n}$) for each steel type is plotted in Fig. 2, which also summarizes the nominal yield stress values. This ratio varies from an average minimum of 1.1 for US A572 Gr.50 steel to an average maximum of 1.4 for Japanese SS400 steel. The values are consistent with the material overstrength values reported in ANSI/AISC 341-16 (AISC 2016a) for US steel grades, the OPUS[1] program (Braconi et al. 2013) for European steel grades, and in Fujisawa et al. (2013) for Japanese steel grades. The measured 28-day concrete compressive strength of the concrete slabs varies between 15 to 40 MPa. In summary, the composite steel beam database is publicly available online at http://resslabtools.epfl.ch/steel.

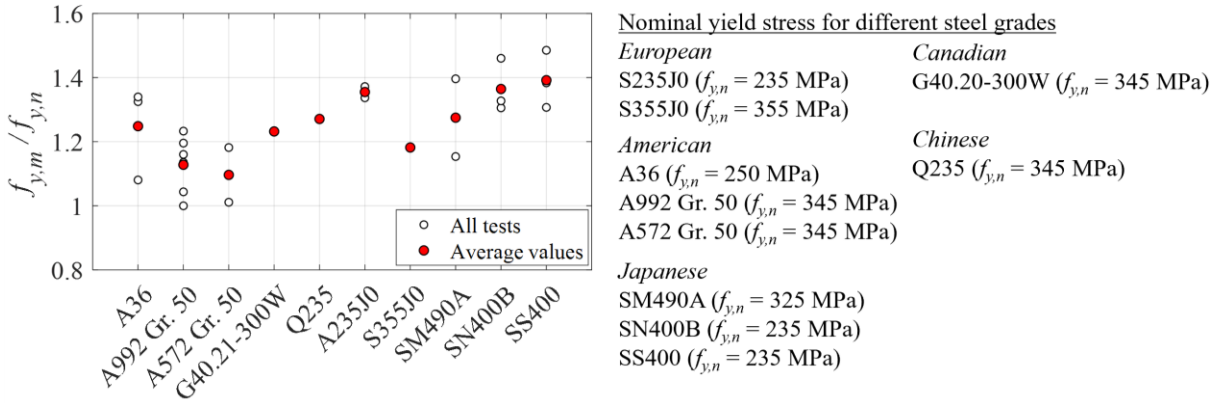

Fig. 2. Ratio of measured-to-nominal yield stress of the various steel types in the assembled database

[1] Optimizing the seismic performance of steel and steel-concrete structures by standardizing material quality control

Table 1. Summary of the composite steel beam testing programs in the assembled database

Reference	Connection Type	h [mm]	Floor Slab*	Steel Grade	$\frac{L_o}{h}$	$\frac{c}{t_w}$
Zhang et al. (2004)	RBS	760/911	NWC - ||	A572/A992 Gr. 50	4.4/5.5	51.9/47.6
Chen and Chao (2001)	RBS	600	NWC - ||	A36	4.4	44.2
Civjan et al. (2001)	Retrofit	755	LWC - ⊥	A36	4.6	51.5
Leon et al. (1998)	WUF-W	683	NWC - ||	A36	4.9	48.6
Engelhardt et al. (2000)	RBS	911	NWC - ||	A572 Gr. 50	3.9	51.9
Tremblay et al. (1997)	RBS	535	NWC - ⊥	G40.21-300W	6.8	45.7
Ricles et al. (2002)	WUF-W	911	NWC - ||	A572 Gr. 50	4.7	51.9
Cheng et al. (2007)	CFT	450	NWC - ||	not reported	6.3	44.0
Cheng and Chen (2005)	RCS	596	NWC - ||	not reported	4.5	53.8
Uang et al. (2000)	Retrofit	911	LWC - ⊥	A36	3.4	51.9
Kim et al. (2004)	TD	612	NWC - SS	SM490	5.4	41.5
Yamada et al. (2009)	TD	400	NWC - ||	SN400B	5.9	43.5
Nakashima et al. (2005)	TD	400	NWC - ||	A572 Gr. 50	7.1	38.0
Nakashima et al. (2007)	TD	400	NWC - ||	SN400B	5.8	38.0
Cordova & Deierlein (2005)	RCS	600	NWC - NR	A572 Gr. 50	5.3	47.8
Bursi et al. (2009)	RCS	400	NWC - ||	S355	5.9	38.5
Kishiki et al. (2010)	TD	300	NWC - SS, ||, ⊥	SM490A/SN400B	5.4	39.4
Sumner & Murray (2002)	BEEP	600	NWC - ||	A572 Gr. 50	5.2	50.6
Bursi et al. (2009)	WUF-W	330	NWC - ||	S235	11.6	36.1
Kim and Lee (2017)	Retrofit	500	NWC - ⊥	SS400	7.6	44.2
Lee et al. (2016)	WUF-W/RBS	350	NWC - ⊥	SS400	6.0	51.3
Lu et al. (2017)	RBS	350	NWC - SS	Q235	4.3	43.1
Asada et al. (2015)	TD	400	NWC - ⊥	SS400	10.6	43.5
Del Carpio et al. (2014)	RBS	350	NWC - ||	A572 Gr. 50	6.0	48.1

*NWC: Normal-weight concrete
LWC: Light-weight concrete
SS: Solid slab with no steel deck
\|\|: Deck with ribs parallel to the beam
⊥: Deck with ribs perpendicular to the beam

3. Deduced Performance Parameters of Composite Steel Beams under Cyclic Loading

A number of performance parameters are deduced from manually digitized and processed moment-rotation relations of the collected data-set. An example is illustrated in Fig. 3. In this figure, the *moment* corresponds to that at the idealized center of the beam's plastic hinge region. The *rotation* represents the beam's rotation over its length (chord rotation). These definitions are consistent with those found in ASCE/SEI 41-17 (ASCE 2017). Referring to Fig. 3a, a first-cycle envelope curve is first fitted to the moment-rotation relation data in both the positive (i.e., sagging bending) and negative (i.e., hogging bending) loading directions. These curves are then used to deduce a number of parameters that characterize the stiffness, flexural strength and plastic deformation capacity of a composite beam. The deduced parameters include the effective stiffness ($K^{+/-}$), the effective plastic flexural resistance ($M_y^{*,+/-}$), the ultimate flexural resistance ($M_u^{+/-}$), and the pre- and post-capping plastic rotation capacities ($\theta_p^{*,+/-}$ and $\theta_{pc}^{*,+/-}$, respectively). The star (*) superscrpit denotes that these parameters are based on the first-cycle envelope curve. Therefore, they are distinguished from those that define a monotonic backbone of a steel beam. The effective stiffness is systematically derived from the unloading stiffness of the first inelastic cycle excursion, which by definition includes both flexural and shear deformations; thus, the term "effective" is adopted. The flexural resistance and rotation parameters are deduced from a tri-linear idealized curve (see dashed lines in Fig. 3b) fitted to the first-cycle envelope. The idealized curve is fitted such that the total energy dissipated up to the peak response

($M_u^{+/-}$) is the same as that in the tri-linear approximation. Albeit the extracted plastic rotation values are loading-history dependent (Krawinkler 2009), they are consistent with prior related studies (Panagiotakos and Fardis 2001) that are already adopted in Eurocode 8-Part 3 (CEN 2005a) and ASCE (2017). The subsequent sections provide a comprehensive assessment of the deduced performance parameters in comparison with relevant seismic code design provisions and performance assessment guidelines for nonlinear static analysis procedures.

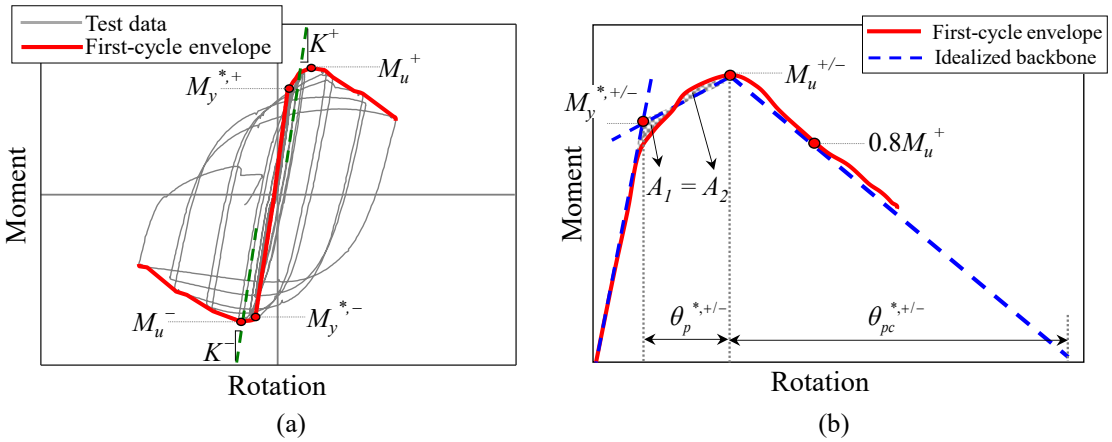

Fig. 3. Definition of performance parameters for composite steel beams under cyclic loading

3.1. Sagging Resistance

The deduced effective plastic flexural resistance of composite steel beams under sagging bending (simply noted as sagging resistance hereafter) is assessed based on 46 data points. These represent beams that reached their ultimate flexural resistance. Beams that experienced premature fracture were excluded from the data-set. The test data suggests that the sagging resistance amplification due to the composite action is mainly dependent on the beam depth, the shear span-to-depth ratio and the degree of composite action, η, which is defined in Eq. (1). In particular, η is the ratio of the actual number of used shear studs to that required ones to achieve full composite action.

$$\eta = \frac{\sum F_v}{\min\{F_c, N_{pl}\}} \leq 1 \tag{1}$$

in which $\sum F_v$ is the shear strength of the headed shear studs between the point of maximum positive moment and the point of zero moment based on the respective code, F_c is the compressive strength of the slab at the crushing limit state, and N_{pl} is the tensile plastic resistance of the steel section based on measured material properties.

The aforementioned dependencies are assessed by plotting the sagging resistance with respect to the aforementioned parameters. The sagging resistance is normalized with respect to the bare steel beam's expected plastic flexural resistance, $M_{p,e}$ ($M_{p,e}$ is the product of the plastic section modulus of the respective beam about the strong axis and the expected yield stress of the beam steel material, $f_{y,e}$). the $f_{y,e}$ is deduced based on the material's expected-to-nominal yield stress ratio, R_y, which is obtained from ANSI/AISC 341-16 (AISC 2016a) for North American steel grades and from available literature (Hirofumi and Masayuki 1985; Braconi et al. 2013; Fujisawa et al. 2013) for the rest of the steel grades.

Figure 4a shows that the sagging resistance is amplified by 13%, on average, for deep beams ($h > 500$ mm). On the other hand, the sagging resistance of shallow composite steel beams ($h \leq 500$ mm) is amplified somewhere between 60% to 80%. This should be carefully considered in the SCWB criterion. Vis-à-vis the above discussions, system-level tests (Suita et al 2008) and supplemental system-level simulations (Lignos et al. 2013) suggest that when the slab contribution is disregarded, the prediction of soft-story collapse mechanisms due to potential drift concentation may be missed.

Referring to Fig. 4b, the sagging resistance of a beam increases when the degree of composite action, η increases. Due to brevity, the η values in Fig. 4b are only computed based on the European provisions (CEN 2004a, b). Note that η varies between codes due to differences in the recommended stud's shear resistance and slab's effective width. This issue is discussed later on in great detail. It is worth noting that deep steel MRF beams may require a large number of shear studs to develop full composite action. However, a lesser number of shear studs is typically used in the actual design phase. In

the context of the U.S. seismic provisions, a lower degree of composite action is actually desirable, considering that the AISC provisions (AISC 2016a) recommend that the SCWB ratio shall be just larger than 1.0.

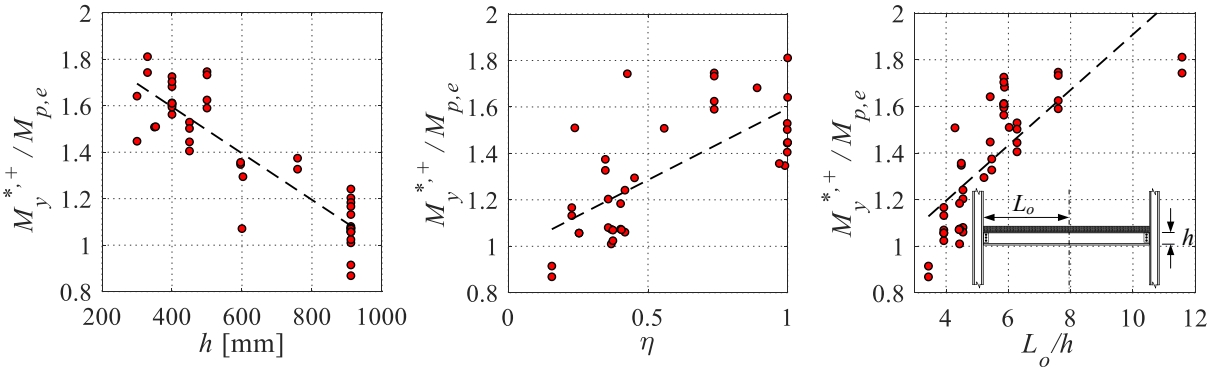

Fig. 4. Dependence of the sagging resistance on the beam's (a) depth, (b) the degree of composite action based on Eurocode provisions (CEN 2004a, b) and (c) span-to-depth ratio

Figure 4c shows that composite steel beams with low L_o/h ratio (mainly deep beams) have a higher moment-shear interaction, which in turn decreases the beam's attained sagging resistance. Notably, although a number of composite steel beams had a $L_o/h < 5$, only two specimens did not develop their bare steel plastic resistance $M_{p,e}$. This suggests that the $L_o/h > 5$ limit specified by ANSI/AISC 358-16 (AISC 2016c) for prequalified beam-to-column connections is rational. Fig. 5 shows the maximum shear demand on the beam, V_u, with respect to L_o/h. The shear demand, V_u, is normalized with respect to the plastic shear resistance, $V_{p,m}$, of the bare steel beam, based on the measured yield stress. Albeit the shear demand on the beam under sagging becomes maximum, V_u values are plotted for both sagging and hogging bending (i.e., V_u^+ and V_u^-, respectively). All but one specimen experienced a $V_u/V_{p,m}$ ratio less than 0.5. This implies that the moment-shear interaction was not relevant in most cases, which complies with the Eurocode seismic provisions. Ten beams experienced a $V_u/V_{p,m}$ ratio larger than 0.4. These beams do not comply with the L_o/h prequalification limits of ANSI/ASCI 358-16 (AISC 2016c).

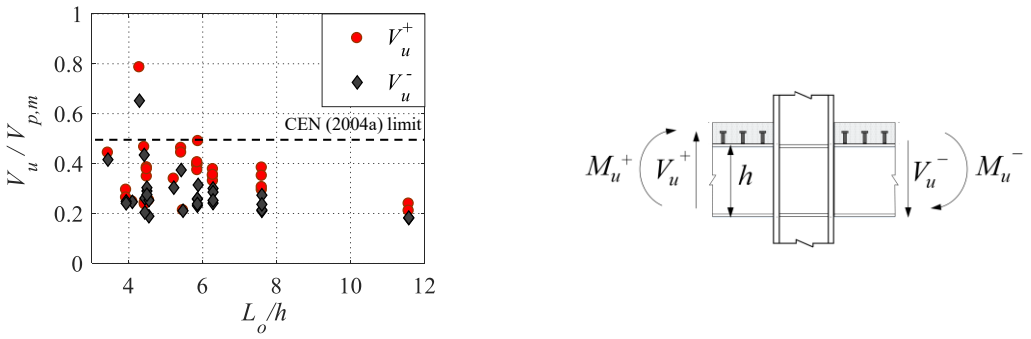

Fig. 5. Dependence of maximum shear demand-to-shear resistance ratio on the beam's span-to-depth ratio

3.1.1. Assessment of the Code-Based Sagging Resistance of Composite Steel Beams

With respect to the design sagging resistance, discrepancies between the design codes are limited to (i) the assumed effective width and compressive stress of the slab and (ii) the assumed shear stud resistance. In this context, a brief discussion of these differences is provided below.

Slab's Effective Width and Compressive Stress

An illustration of the basic dimensions used for effective width calculations by the three codes as well as a tabulated comparison of the formulas used for these calculations are shown in Fig. 6a and 6b, respectively. The general consencus is that the effective width calculation as per the U.S. and Japanese provisions is simpler than that of the European provisions. For instance, the effective width according to the Eurocode provisions differs depending on (i) the loading condition (gravity/seismic), (ii) the joint configuration (exterior/interior column), and (iii) the presence of transverse beams or

anchored rebar in the slab. The Japanese provisions simply recommend an effective width equal to the column flange width. This agrees with past findings from Du Plessis and Daniels (1972) but it is a conservative assumption in most cases.

For the concrete slab's design compressive stress, both the European (CEN 2004b) and American (AISC 2016b) provisions consider 85% of the concrete specified/characteristic compressive strength. This value is rational for partially-composite steel beams (Civjan et al. 2001; Cordova and Deierlein 2005). On the other hand, the Japanese provisions consider twice the compressive strength for fully composite steel beams, in which the effective stress can reach up to $1.8f'_c$. This is consistent with observations from past studies (Du Plessis and Daniels 1972; Tagawa et al. 1989).

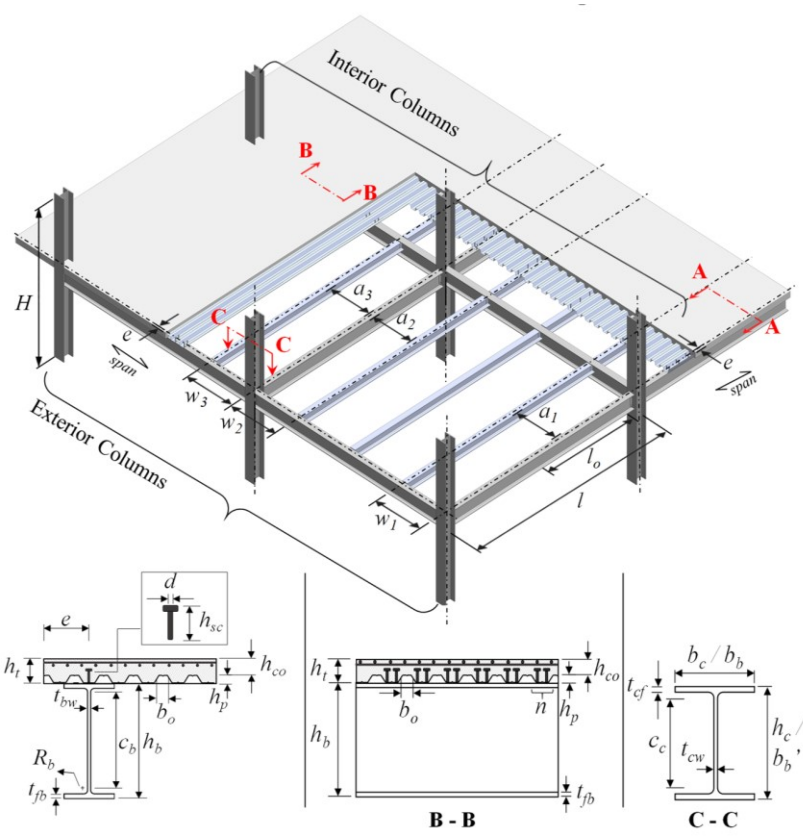

(a)

Code	Effective width*	
	Interior column	Exterior column
CEN (2004a)	$\min\{0.075l;\ e\}$	(1) $\min\{0.075l;\ e\}$ (2) $\min\{0.5(b_b+0.7h_c);\ e\}$ (3) $\min\{0.5(b_b'+0.7h_c);\ 0.05l;\ e\}$
AISC (2016a)	$\min\{0.0125l;\ w;\ e\}$	
AIJ (2010a)	b_b	

* Effective width on each side of the beam web centerline
(1) Transverse beams with stud connectors and column strong axis oriented in loading direction. Concrete slab up to exterior face of column or beyond
(2) Same as (1) but without steel transverse beams or steel transverse beams without stud connectors
(3) All other layouts

(b)

Fig. 6. (a) Illustration of frame and composite steel beam dimensions for effective width computations; and (b) comparison of code-based effective width for plastic analysis

Shear Resistance of Headed Studs

Both Eurocode 4-Part 1 (CEN 2004b) and ANSI/AISC 360-16 (AISC 2016b) reduce the stud's shear resistance in the presence of a steel deck, regardless of its orientation. The Japanese provisions (AIJ 2010a) only consider this reduction if the steel deck ribs are oriented perpendicular to the steel beam. In general, the reduction factor is a function of the deck and stud dimensions. If the steel deck is oriented perpendicular to the beam, this factor becomes also dependent on the number of studs per rib. The U.S. (AISC 2016a) and European (CEN 2004a) provisions require an additional 25% reduction on the shear resistance of headed studs in seismic load resistant systems.

Comparison of Code-based and Test-based Sagging Resistances

The design sagging resistance, M_d^+, is calculated here using plastic analysis as adopted in the three considered design provisions. Figure 7a shows the ratios of test- to code-based sagging resistance, $M_y^{*,+}/M_d^+$, versus the beam depth. The trend lines suggest that the Eurocode tends to overestimate the sagging resistance of deep beams ($h \approx 900$ mm). This is due to the assumed constant material overstrength factor of 1.25, regardless of the steel material type. The collected deep beams are mainly made of A992 Gr.50 steel. This has a lower material overstrength ($R_y = 1.1$). This issue as well as the observed variability in the M_d^+values diminish between the three codes when the measured yield stress is used to calculate the design

sagging resistance, $M_{d,m}^{+}$ (see Fig. 7b). Thus, the material overstrength shall be related to the steel grade (refer to Fig. 2) as adopted in ANSI/AISC 341-16 (AISC 2016a). In a similar manner, the proposed material overstrength values from the OPUS program (Braconi et al. 2013) can be adopted in future editions of Eurocode 8. It is also worth noting that the Japanese steel industry addressed this issue by developing new steel grades with specified upper and lower limits on the yield stresss (Nakashima et al. 2000; Kanno 2016).

The findings also suggest that the sagging resistance is not sensitive to the rest of the aforementioned differences between design codes. Therefore, the ANSI/AISC approach (AISC 2016a, b) is recommended for the computation of the stud's shear resistance given its simpler formulation. Since the sensitivity of the results to variations in the slab's effective width is also negligible, the detailed approach of Eurocode 8-Part 1 (CEN 2004a) is not justifiable. Alternatively, either the AISC (2016a, b) or the AIJ (2010a) approaches are recommended for future revisions of Eurocode 8-Part 1.

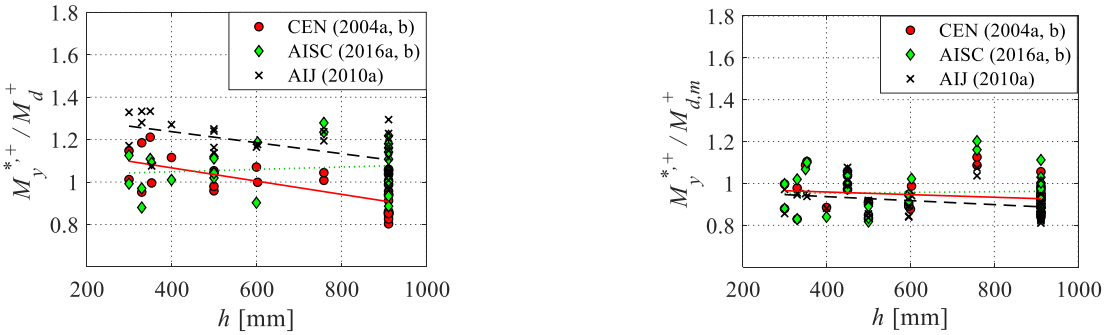

Fig. 7. Test- to code-based sagging resistance ratio versus beam depth based on (a) expected material properties according to respective code; and (b) measured material properties

3.2. Hogging Resistance

Fig. **8** shows the ratio of the test-based hogging resistance to the expected bare steel beam plastic resistance ($M_p^{*,+}/M_{p,e}$) versus the beam depth. The test-based hogging resistance is, on average, 10% higher than $M_{p,e}$. This is consistent with prior observations by Elkady and Lignos (2014). This amplification is attributed to contributions from the slab longitudinal reinforcement and the metal deck. This becomes more evident in shallow beams. Note that the majority of the collected tests includes reinforced slabs with a steel wire mesh (reinforcement area less than 5 mm^2/cm slab width). Interestingly, shallow beams (h = 300 ~ 330 mm) with relatively high deck reinforcement (8~13 mm^2/cm), that were tested by Bursi and Gramola (2000) and Kishiki et al. (2010), developed the largest amplification factors of 1.4 to 1.5 as highlighted in Fig. 8.

Most of the collected reports did not indicate the exact location of the slab reinforcement including their measured yield stress. Therefore, it was possible to calculate the design hogging resistance, $M_{d,m}^{-}$ for only eight of the collected specimens. The ANSI/AISC 360-16 (AISC 2016b) allows for the consideration of the slab reinforcement within the sagging plastic effective width (see Fig. 4b) while the Eurocode 8 (CEN 2004a) distinguishes between the effective width under sagging and hogging bending. However, the average ratio, $M_y^{*,-}/M_{d,m}^{-}$, is found to be 0.97 and 0.96 for the AISC (2016a, b) and Eurocode (CEN 2004a, b), respectively. This implies that the sensitivity of the hogging resistance to the slab effective width variation is negligible. Therefore, it is rational to adopt the simpler ANSI/AISC 360-16 (AISC 2016b) approach for the effective width computations in future editions of Eurocode 8-Part 1.

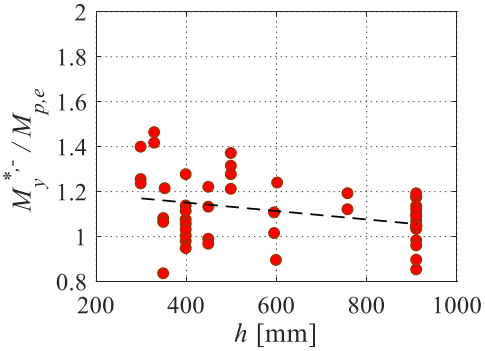

Fig. 8. Normalized test-based hogging resistance versus beam depth

3.3. Effective Stiffness

The effective stiffness under sagging (K^+) and hogging (K^-) bending is plotted versus the beam depth in Fig. 9a and 9b, respectively. In this figure, the test-based stiffness is normalized by the theoretical stiffness of the non-composite steel beam, K_{nc}, considering both flexural and shear deformations. The test-based effective stiffness could only be obtained for 29 specimens; those are the ones where the beam's moment-rotation relation could be deduced from the reported test data.

Fig. 9a shows that the composite action amplifies the effective stiffness of shallow beams ($h \leq 500$mm) under sagging bending by up to 100%. This agrees with findings from system-level experiments (Nakashima et al. 2007; Nam and Kasai 2012). For deep beams ($h > 500$ mm), the effective stiffness increases, on average, by 30%. Referring to Fig. 9b, the effective stiffness under hogging bending is amplified by up to 35% depending on the beam depth and the amount of slab reinforcement as discussed earlier. For few specimens, the K^-/K_{nc} values are slightly less than 1.0, which is attributed to the sensitivity of K^- deduction from the test data. The effective stiffness is also dependent on the degree of composite action as discussed in the subsequent section.

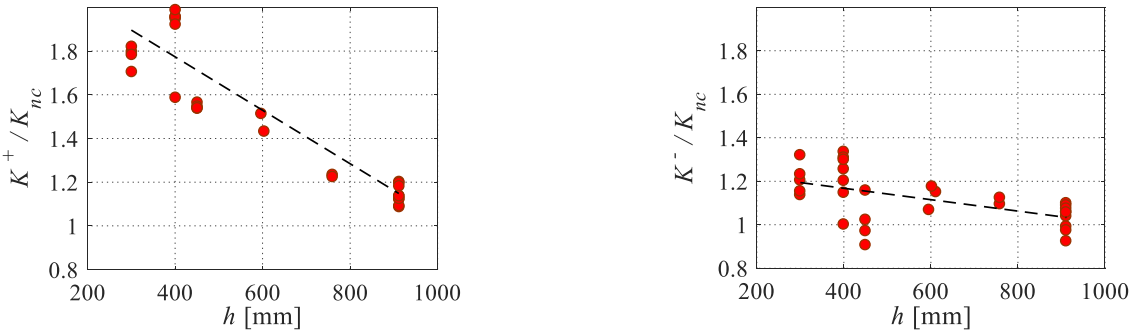

(a) Sagging bending (b) Hogging bending

Fig. 9. Dependence of the composite steel beam's effective stiffness on its depth

3.3.1. Assessment of Code-based Effective Stiffness under Sagging Bending

The three codes calculate the effective stiffness under sagging bending, based on the effective moment of inertia of the un-cracked fully-composite cross-section. The level of accuracy of these code estimates, that generally involve design-related reduction factors depending on a target limit state, is assessed here based on the deduced (i.e., actual) stiffness measurements of the collected test data (see Fig. 3). Section C-13 commentary of the ANSI/AISC 360-16 (AISC 2016b) as well as the Japanese (AIJ 2010a) provisions employ Eq. (2) to estimate the moment of inertia for partially-composite steel beams, I_{pc}, in which, I_{nc}, and I_c are the moments of inertia of the non-composite and fully composite steel beams, respectively.

$$I_{pc} = I_{nc} + \sqrt{\eta}(I_c - I_{nc}) \tag{2}$$

The ANSI/AISC 360-16 (AISC 2016b) recommends an additional 25% reduction in the composite beam's moment of inertia for realistic deflection calculations (Leon 1990; Leon and Alsamsam 1993). For the same purpose, the Japanese provisions (AIJ 2010a) use a larger modular ratio, n = 15 (defined as the ratio of the steel-to-concrete elastic modulus). Based on Eq. (2), the effective moment of inertia depends on the assumed slab effective width, which in turn differs in the elastic and plastic ranges. In the former, the effective width is related to the shear lag phenomenon (Castro et al. 2007). In the latter, stress redistribution in the slab occurs due to material nonlinearity, which increases the corresponding slab effective width. Accordingly, different effective widths shall be assumed for the plastic flexural resistance and the serviceability calculations (stiffness and deflection checks). Table 2 summarizes a comparison of the effective widths proposed by the three design codes for elastic analysis. In summary, Eurocode 8 considers a smaller slab effective width for elastic analysis than for plastic flexural resistance calculations. The effective width, as per Eurocode 8, is also dependent on the column configuration as well as the presence of transverse beams and anchored rebar in the slab (CEN 2004a). The ANSI/AISC 360-16 (AISC 2016b) provisions do not distinguish between elastic and inelastic analysis. The Japanese design recommendations propose a different effective width for elastic analysis that depends on the beam span. Both Eurocode 8 and Japanese provisions propose a fixed value for the modular ratio, n.

Figure 10 shows the ratio of the test- to code-based effective stiffness under sagging bending, K^+/K_d^+ versus the beam depth and degree of composite action. It appears that the 25% reduction imposed on I_{pc} by AISC (2016a, b) for realistic

deflection calculations results in a conservative estimate of the effective stiffness. However, long term effects, may actually reduce the effective stiffness of composite steel beams over a building's life-cycle. This effect cannot be assessed here since, in most cases, the collected tests were conducted within one month after concrete casting.

Table 2. Summary comparison of code-based effective width computation for elastic analysis

Code	Effective width*		Modular ratio, n
	Interior column	Exterior column	
CEN (2004a)	$\min\begin{cases}0.0375l\\ e\end{cases}$	$^{(1)}\min\begin{cases}0.0375l\\ e\end{cases}$ $^{(2)}\min\begin{cases}0.025l\\ e\end{cases}$	7
AISC (2016b)	$\min\begin{cases}0.0125l\\ w\\ e\end{cases}$		E_s/E_c
AIJ (2010b)	$\min\begin{cases}b+(0.5-0.6a/l)a & \text{if } a<0.5l\\ b+0.1l & \text{if } a\geq 0.5l\end{cases}$		15

* Effective width on each side of the beam web centerline
(1) With transverse beams and anchored rebars
(2) Without transverse beams or rebars not anchored
b = Flange width/2 for symmetric slab configuration.
= Flange width for asymmetric slab configuration.

In brief, the Eurocode and Japanese provisions provide close estimates of the effective stiffness with an average K^+/K_d^+ values of 0.96 and 0.91, respectively. The associated coefficient of variation (COV) is 0.12 and 0.06 for the Eurocode and Japanese data points, respectively. The higher dispersion based on the Eurocode is attributed to the fact that it always assumes a fully composite cross-section; thus the Eurocode is conservative for beams with lower degree of composite action ($K^+/K_d^+ < 0.85$, see Fig. 10b) as well as for fully-composite shallow beams ($K^+/K_d^+ > 1$).

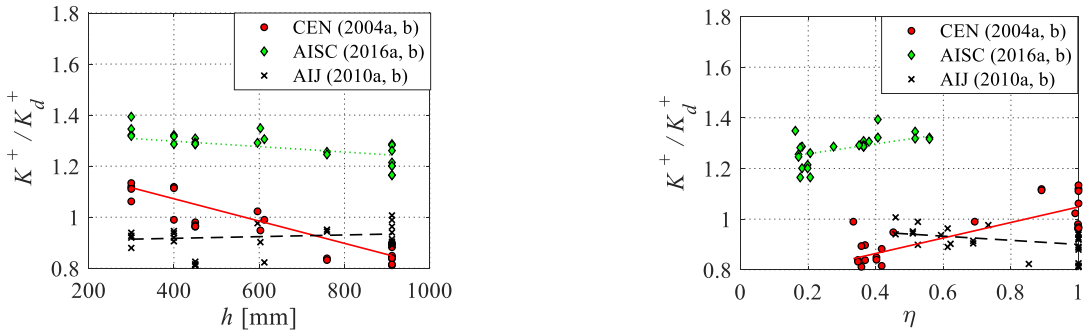

(a) beam depth (b) degree of composite action

Fig. 10. Ratio of test- to code-based sagging effective stiffness

3.4. Plastic Rotation Capacity of Composite Steel Beams

The assembled database is used to quantify the pre- and post-capping plastic rotation capacities of composite steel beams, under sagging and hogging bending and to propose empirical equations for predicting these quantities. These equations can be used in the context of seismic assessment guidelines for new and existing steel frame buildings.

Eurocode 8-Part 3 (CEN 2005a) simply predicts a plastic rotation ($\theta_{p,pred}$) equal to $8\theta_y$ and $3\theta_y$ for Class 1 and 2 cross-sections, respectively (where θ_y is the chord rotation at yielding) for non-composite steel beams. These values are anchored to the near-collapse limit state (Panagiotakos and Fardis 2001), which corresponds to the plastic rotation capacity at 20% drop in the beam's peak flexural resistance.

Using experimental data collected by Lignos and Krawinkler (2011, 2013), Hartloper and Lignos (2017) developed empirical equations to predict the pre- and post-capping plastic rotation of non-composite beams based on their first cycle envelope curve as defined in Fig. 3b. These equations are further refined here by supplementing the collected experiments with data from non-composite steel beams that were conducted mostly in Europe. The equations are developed through

standard multiple regression analysis (Chatterjee and Hadi 2015). The refined expressions are provided for θ_p^* and θ_{pc}^* as defined in Fig. 3. In particular, for standard non-composite steel non-RBS beams,

$$\theta_p^* = 0.25 \cdot \left(\frac{c}{t_w}\right)^{-0.9} \cdot \left(\frac{b}{2t_f}\right)^{-1.1} \cdot \left(\frac{L_b}{i_z}\right)^{-0.2} \cdot \left(\frac{L_o}{h}\right)^{1.1} \cdot \left(\frac{E}{f_{y,e}}\right)^{0.2} \quad (COV = 0.38) \tag{3}$$

$$\theta_{pc}^* = 12.67 \cdot \left(\frac{c}{t_w}\right)^{-0.9} \cdot \left(\frac{b}{2t_f}\right)^{-0.9} \cdot \left(\frac{L_b}{i_z}\right)^{-0.5} \cdot \left(\frac{E}{f_{y,e}}\right)^{0.1} \quad (COV = 0.44) \tag{4}$$

and for non-composite steel beams with RBS,

$$\theta_p^* = 0.12 \cdot \left(\frac{c}{t_w}\right)^{-0.5} \cdot \left(\frac{b}{2t_f}\right)^{-0.7} \cdot \left(\frac{L_b}{i_z}\right)^{-0.5} \cdot \left(\frac{L_o}{h}\right)^{0.8} \cdot \left(\frac{E}{f_{y,e}}\right)^{0.23} \quad (\text{COV} = 0.42) \tag{5}$$

$$\theta_{pc}^* = 4.91 \cdot \left(\frac{c}{t_w}\right)^{-1.1} \cdot \left(\frac{b}{2t_f}\right)^{-0.1} \cdot \left(\frac{L_b}{i_z}\right)^{-0.1} \cdot \left(\frac{E}{f_{y,e}}\right)^{0.09} \quad (\text{COV} = 0.47) \tag{6}$$

In which, L_b is the unbraced length of the beam, i_z is the weak-axis' radius of gyration, E and $f_{y,e}$ are the steel's modulus of elasticity and expected yield stress, respectively. The above equations are valid within the following ranges: $35 \le c/t_w \le 55$, $3 \le b/2t_f \le 8$, $20 \le L_b/i_z \le 80$ (RBS: $20 \le L_b/i_z \le 60$), $3 \le L_o/h \le 8$ (RBS: $5 \le L_o/h \le 8$), $440 \le E/f_{y,e} \le 830$.

To assess the predicted plastic rotation capacities based on the proposed Eqs. (3) to (6) as well as the Eurocode 8 approach, the pre- and post-capping plastic rotations under sagging and hogging bending are deduced from the gathered experimental data. To be consistent with the Eurocode 8 definition, the plastic rotation at 20% drop in peak flexural resistance, $\theta_{p,80\%M_u}^{*,+/-}$, is deduced from the test data. The same is done to deduce the predicted plastic rotation capacities corresponding to 80% $M_u^{+,-}$ based on Eqs. (3) to (6). In particular, $\theta_{p,pred} = \theta_p^{*,+/-} + 0.2\ \theta_{pc}^{*,+/-}$. The ratio of test-based to predicted plastic rotation, $\theta_{p,80\%M_u}^{*,+/-}/\theta_{p,pred}$, ratio versus the beam's web slenderness ratio (c/t_w) is plotted in Fig. 11. The web slenderness ratio is used here since steel beams in fully restrained beam-to-column connections are mainly prone to web local buckling followed by flange buckling (Lignos and Krawinkler 2011). Also note that data points in this figure exclude tests where beams experienced premature fracture or those terminated prior to reaching 80% M_u.

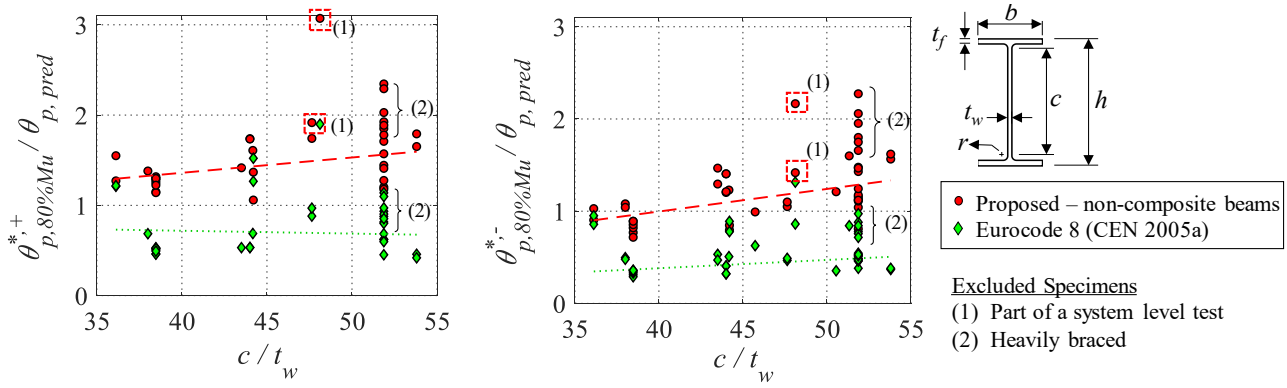

(a) Sagging bending (b) Hogging bending

Fig. 11. Ratio of test-based to predicted plastic rotation at 20% flexural strength loss with respect to beam's web slenderness

Referring to Fig 11a and 11b, the plastic rotation capacity under sagging bending is generally larger than that under hogging bending. This is due to the lateral restraint provided by the slab to the steel beam's top flange and top portion of the web, thereby delaying the top flange local buckling. Moreover, Eurocode 8-Part 3 consistently overestimates the plastic rotation capacity under both sagging and hogging bending by about 50%, regardless of the c/t_w and degree of composite action, η. This agrees with prior related studies (Araújo et al. 2017). The main reason is that this approach ignores the influence of geometric and material properties of a steel beam on its plastic rotation capacity. Referring to Fig. 11b, for hogging bending, the plastic rotation predicted based on Eqs. (3) to (6) matches the measured one relatively well. Under sagging bending, the refined equations underestimate $\theta_{p,80\%M_u}^{*,+}$ by almost a constant value of 1.5. This is expected since these equations are meant for non-composite beams. The larger scatter around the predicted plastic rotation values at $c/t_w \approx$

52 is attributed to differences in lateral stability bracing between the collected tests. In fact, several of the collected specimens were heavily braced such that the predominant instability would be cross-sectional local buckling. Based on these observations, for composite steel beams under sagging bending, $\theta^{*,+}_{p,80\%M_u}$=1.5 $\theta_{p,pred}$ as per Eqs. (3) to (6) depending on the beam-to-column connection type. Similarly, under hogging bending, $\theta^{*,-}_{p,80\%M_u}$= $\theta_{p,pred}$.

Interestingly, one test specimen (highlighted in Fig. 11) achieved a much larger $\theta^{*,+/-}_{p,80\%M_u}$ of 7.8% and 5.5% rad under sagging and hogging bending, respectively. This corresponds to an interior beam as part of a system-level test (Del Carpio et al. 2014). Cordova and Deierlein (2005) found that the axial restraint provided by the slab continuity in composite steel concrete MRFs increases the plastic rotation capacity of interior joint beams. This is not captured in the majority of the available experimental data due to their simplified boundary conditions (Roeder 2000). The authors are currently investigating this issue more thoroughly in a separate study.

The post-capping plastic rotation is deduced from 13 and 25 tests under sagging and hogging bending, respectively. The deduced $\theta_{pc}^{*,+/-}$ values are normalized with respect to the post-caping rotation predicted by Eqs. (4) and (6) and plotted versus c/t_w in Fig. 12. Note that Eurocode 8-Part 3 does not provide estimates for this quantity. The data trends suggest that the influence of the concrete slab on the post-capping plastic rotation is not as pronounced as on $\theta^{*,+/-}_{p,80\%M_u}$. This agrees with prior findings by Elkady and Lignos (2014). Under sagging bending, the post-capping plastic rotation is about 20% larger than that predicted for the non-composite beam (see Fig. 12a). Under hogging bending (see Fig.12b), $\theta_{pc}^{*,-}$ is, on average, 10% lower than that predicted by the regression equations for non-composite steel beams. Under hogging bending, a bigger portion of the steel cross-section is under compression, which increases the potential for local and/or lateral torsional buckling (PEER/ATC 2010). In conclusion, it is recommended that for composite steel beams under sagging bending, the post-capping plastic rotation shall be taken as 1.2 times θ_{pc}^{*} of non-composite beams as per Eqs. (4) and (6). Under hogging bending, the post-capping plastic rotation shall be computed directly from Eqs. (4) and (6).

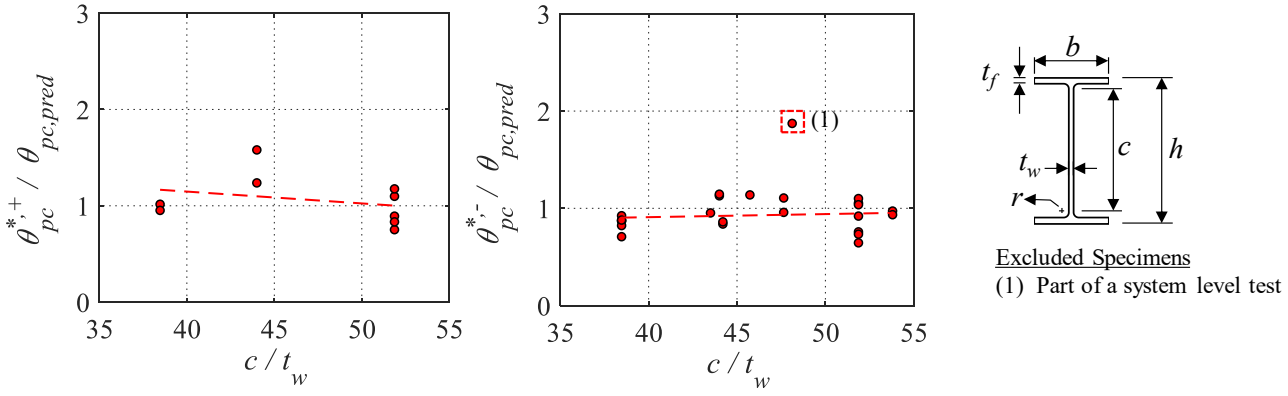

(a) Sagging bending (b) Hogging bending

Fig. 12. Ratio of test-based to predicted post-capping plastic rotation with respect to the beam's web slenderness

4. Influence of Composite Action on Beam-to-Column Web Panel Zone

The shear demand on the beam-to-column web panel zone of 45 composite steel beams is deduced and assessed with respect to the web panel shear resistance computed by the American, European and Japanese steel design specifications (CEN 2005c; AIJ 2010a; AISC 2016b). Referring to Fig. 13, based on the equilibrium of the external forces at a given joint, the maximum shear demand on the panel zone, $V_{PZ,demand}$, is deduced from the tests as follows,

$$V_{PZ,demand} = \frac{M_u^+}{d_{eff}^+} + \frac{M_u^-}{d_{eff}^-} - V_{col} = \frac{M_u^+}{d_{eff}^+} + \frac{M_u^-}{d_{eff}^-} - \frac{M_u^+ + M_u^-}{H} \cdot \frac{l}{l - h_c} \tag{7}$$

in which, M_u^+ and M_u^- are the peak sagging and hogging bending demands at the column face, respectively, d_{eff}^+ and d_{eff}^- are the effective panel zone depths for sagging and hogging bending, V_{col} is the shear force in the column, l and H are defined in Fig. 6a. Note that M^- is zero for exterior joints. Under hogging bending, the effective depth d_{eff}^- is equal to the bare steel beam depth, h. Under sagging bending, the top flange resultant force shifts towards the slab and the resulting d_{eff}^+ is deduced by Eq. (8) that considers the concrete slab geometry (Kim and Engelhardt 2002; Elkady and Lignos 2014),

$$d_{eff}^{+} = h + h_t - 0.5h_c - 0.5t_{bf} \tag{8}$$

Generally, the yield shear resistance of the panel zone, V_y, is expressed by Eq. (9), in which A_v is the shear area of the panel zone, f_{yv} is the shear yield stress (taken as $0.58 \sim 0.6f_{y,n}$), and α is a reduction factor that accounts for the axial load-shear interaction. In the American and Japanese provisions, α depends on the column axial load demand. The axial force-shear interaction is ignored in Eurocode 3 (CEN 2005c). Instead, a flat reduction factor equal to 0.9 is considered. Ciutina and Dubina (2003) stated that this factor accounts for the reduction due to axial load-shear interaction.

$$V_y = \alpha A_v f_{yv} \tag{9}$$

Eurocode 8 allows up to 30% contribution of the panel zone to the joint's total inelastic deformation. The panel zone plastic shear resistance is expressed by Eq. (10) as per ANSI/AISC 360-16 (AISC 2016b) and Eq. (11) as per Eurocode 3, in which, b_c and t_{cf} are the width and thickness of the column flange, respectively; h_b and t_{bf} are the beam's depth and flange thickness, respectively (see Fig. 13). The Japanese code reduces the shear demand by 25%. The joint is then designed for V_y (Nakashima et al. 2000).

$$V_p = V_y\left(1 + 3\frac{b_c t_{cf}^{\,2}}{h_b h_c t_p}\right) \tag{10}$$

$$V_p = V_y + \frac{b_c t_{cf}^{\,2}}{(h_b - 2t_{bf})} f_{y,n} \tag{11}$$

None of the three design provisions suggests how the composite slab shall be considered in the panel zone shear demand and resistance computations. The panel zone's yield and plastic shear resistances are calculated based on the three code provisions based on nominal material properties.

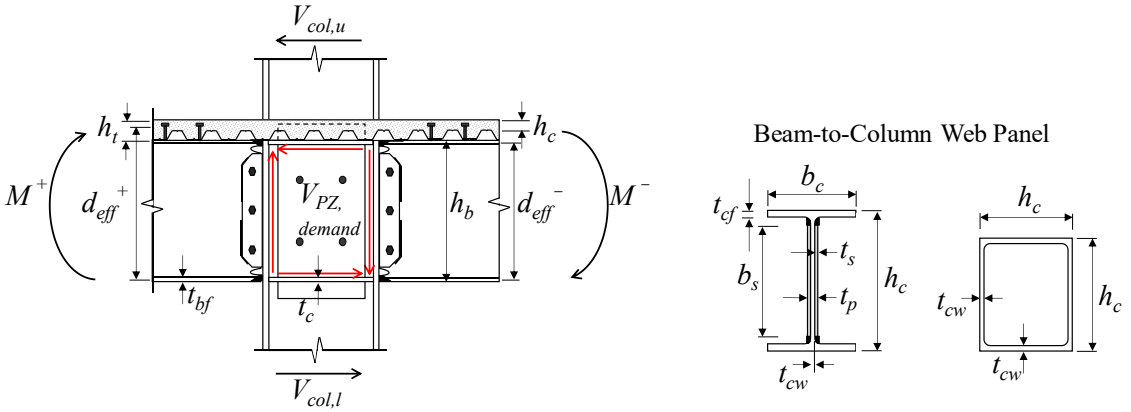

Fig. 13. Panel zone dimensions and definition of the effective depth under sagging and hogging bending

Figure 14a and 14b show the panel zone shear resistance, $V_{PZ,d}$, versus the panel zone shear demand, $V_{PZ,demand}$, for wide-flange and hollow structural section (HSS) columns, respectively. For reference, three dashed lines are superimposed in Fig. 14 that represent a $V_{PZ,d}$ to $V_{PZ,demand}$ ratio of 0.6, 1.0 and 1.67. Also in Fig. 14a, the labeled specimens were intentionally designed for a very strong ('S') or very weak ('W') panel zone. The figure shows that the estimated yield shear resistance based on AISC (2016b) and AIJ (2010a) is between 0.70 to 1.25 times the panel zone shear demand. In total, 14 out of 23 wide-flange specimens experienced a shear demand greater than the yield resistance because the amplified sagging flexural resistance of the composite beam was neglected in design; hence underestimating the shear demand.

The estimated panel zone shear resistance according to Eurocode 3 varied between 0.6 to 1.1 times the corresponding shear demand. The Eurocode approach is particularly conservative for panel zones with doubler plates. This is because i) the Eurocode only considers a single doubler plate thickness even if two plates exist and ii) the panel zone shear resistance includes a 0.9 reduction factor regardless of the imposed axial load demand. All but two specimens experienced a shear

demand greater than the Eurocode-based panel zone shear resistance. This conservatism is due to the associated uncertainty in estimating the panel zone contribution to the plastic rotation demands of the beam-to-column joint (Castro et al. 2008).

Referring to Fig. 14b, about half of the specimens with HSS and built-up box sections experienced a lower demand than the panel zone shear resistance, regardless of the respective code provision. Specimens in which the demand was higher than the code-based yield shear resistance experienced panel zone shear yielding (see Table 3). According to Nakashima et al. (2000), while Japanese limit state design principles encourage panel zone yielding, Japanese buildings are less commonly controlled by panel zone yielding.

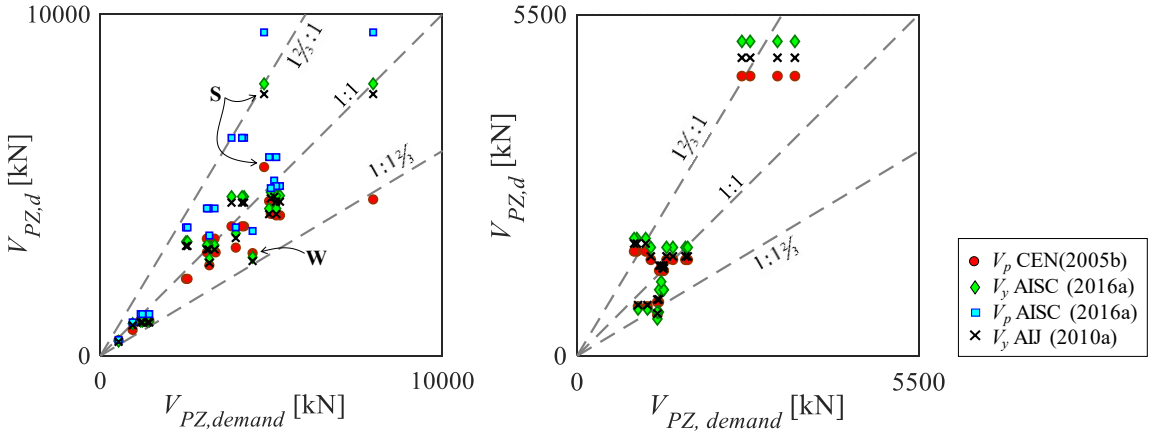

(a) Wide-flange columns (b) HSS and built-up columns

Fig. 14. Code-based panel zone shear resistance versus maximum panel zone shear demand

The gathered experimental data suggest that story drift demands exceeding 5% can be sustained even if the panel zone develops a total shear distortion up to 10 γ_y (≈ 0.023 rad). This can be achieved with a $V_{PZ,d}$ / $V_{pl,b}$ ratio of 0.8. The limit, which is applicable to all three design provisions, is based on the panel zone's yield shear resistance and the plastic flexural resistance of composite steel beams. Because this finding is based on subassembly test data, system-level studies shall be conducted in order to evaluate the influence of controlled inelastic behavior of panel zones on the dynamic response of steel MRFs relative to "strong" panel zone designs. However, this is outside the scope of the present work.

4.1 Recommendations for Panel Zone Shear Resistance

While design provisions allow for controlled inelastic panel zone yielding, there is no clear guidance on the relative panel zone-to-beam shear resistance. For this purpose, specimens for which the panel zone yield deformation was reported are analyzed separately. The collected specimens are summarized in Table 3 along with their reported failure mode. Specimens that fractured prior to a peak story-drift ratio of 5% and those that do not reflect the current design practice according to modern design provisions, are listed in Table 3 but are excluded from the subsequent assessment.

Figure 15 shows the panel zone shear resistance, $V_{PZ,d}$, normalized by $V_{pl,b}$ versus the panel zone total rotation (expressed as multiples of the nominal yield rotation in shear, γ_y). The $V_{pl,b}$ is the shear demand on the panel zone due to the development of the composite beam's plastic flexural resistance. This is calculated according to the respective design provision using the measured material properties to eliminate the material uncertaintly (i.e., $M_{d,m}^+$ and $M_{d,m}^-$ as defined earlier). This measure of the beam's relative shear resistance has been adopted in prior related studies (Roeder 2002; Lee et al. 2005). Note that the calculated beam plastic shear resistance accounts for the presence of the slab and neglects cyclic hardening.

Referring to Fig. 15a, composite connections with wide-flange columns and a $V_{PZ,d}$-to-$V_{pl,b}$ ratio larger than 0.8, attained a shear distortion angle of up to 10γ_y (γ=0.023 rad) without experiencing premature fracture. Lee et al. (2005) found that a $V_{PZ,d}$-to-$V_{pl,b}$ ratio between 1.10 and 1.42 is sufficient for the panel zone to develop a plastic rotation of 0.01 rad. However, the influence of the composite slab was disregarded in this case. When the $V_{PZ,d}$-to-$V_{pl,b}$ ratio is between 1.10 to 1.42, the panel zone develops a rotation of 8.5γ_y; i.e., the plastic rotation is equal to 0.019 rad, which still exceeds 0.01 rad.

Referring to Fig. 15b, for HSS columns, only three data points were collected (Yamada et al. 2009, Kishiki et al. 2010). Although inconclusive, two of these specimens experienced a panel zone shear distrortion more than 15γ_y. Those were through-diaphragm connections with fully-composite shallow beams. The specimen tested Kishiki et al. (2010) had a fully

composite beam with a solid slab. Consequently, the composite beam remained elastic due to the large amplification in the plastic bending resistance and the plastic deformations of the subassembly were mainly concentrated in the panel zone.

Table 3. Composite steel beam specimens with reported panel zone shear distortion

Reference	Specimen ID	Column section	$\frac{\gamma}{\gamma_y}$	Failure Mode	SDR_{max} [%]
Zhang et al. (2004)	SPEC-1	W36x230	4.91	Fracture in RBS bottom flange	5.0
	SPEC-2	W27x194	8.28	Fracture in RBS top flange	5.0
	SPEC-3	W27x194	4.64	Fracture in RBS	5.0
	SPEC-4	W36x150	5.78	Low cycle fatigue cracks	5.0
	SPEC-5	W27x146	7.93	Low cycle fatigue cracks	5.0
Ricles et al. (2002)	C5[(a)]	W14x398	6.67	Fracture in top flange at shear stud in plastic hinge region	2.6 [(b)]
Engelhardt et al. (2000)	DBBWC	W14x398	7.8	Fracture at beam groove weld	6.0
	DBWWC	W14x398	8.40	Ductile tearing through top beam flange	7.0
	DBBWSPZC	W14x398	1.10	No fracture; test terminated	7.0
	DBWWPZC[(a)]	W14x283	23.23	Fracture in beam flange weld and shear-tab-to-column weld	7.0
Uang et al. (2000)	NIST-2C[(a)]	W14x426	2.58	No fracture; test terminated	4.0
Yamada et al. (2009)	Beam 1	HSS300x300x9	18.15	No fracture; test terminated	9.0
	Beam 2[(a)]	HSS300x300x9	3.60	Beam fracture at scallop location	2.5
Kishiki et al. (2010)	F_Full	HSS250x250x9	22.07	No fracture; test terminated	5.0
	D_LS	HSS250x250x12	5.19	No fracture; test terminated	5.0
	D_SS[(a)]	HSS250x250x12	4.84	Beam fracture	3.5
Sumner & Murray (2002)	4E-1.25-1.375-24	W14x257	1.83	Bolt tension rupture	5.0
Kim & Lee (2017)	PN500-C[(a)]	H400x400x13x21	15.17	Fatigue fracture in bottom flange weld	4.0[(b)]
	PN500C-HST[(a)]	H400x400x13x21	28.56	Low cycle fatigue beam fracture	7.0[(b)]
	PN500C-SH	H400x400x13x21	5.42	No fracture	>5.0[(b)]
	PN500C-TH	H400x400x13x21	9.07	No fracture	>5.0[(b)]
Del Carpio et al. (2014)	RBS-A	W12x30	3.81	No fracture; test terminated	16.4

[(a)] Specimens that are excluded from subsequent discussion
[(b)] Total plastic rotation reported instead of story drift ratio

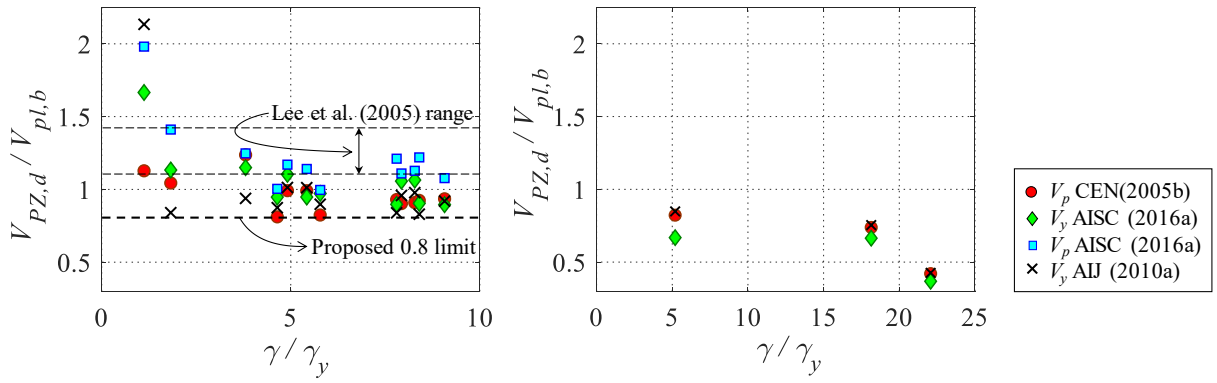

(a) Wide-flange columns (b) HSS columns

Fig. 15. Relative panel-zone-to-beam shear resistance against the normalized panel zone's distortion angle

5. Conclusions

This paper investigates the composite steel beam effects on the seismic design and performance assessment of composite-steel moment resisting frames (MRFs). For this purpose, a publicly available database of 97 composite steel beams was assembled. Several parameters were investigated including the sagging and hogging flexural resistances, the effective stiffness and the plastic rotation capacity of composite steel beams. The influence of the slab on the beam-to-column web panel shear resistance was also investigated. A comparison between the European, American and Japanese provisions was conducted; the aim of which is to provide design recommendations on how to properly consider the composite action in future design code revisions. Empirical formulations were also developed that capture the asymmetric behavior of composite steel beams under cyclic loading. Such relationships can be used in seismic assessment of new and existing steel frame buildings based on nonlinear static (pushover) analysis. The main findings are as follows:

- The sensitivity of the results to discrepancies between the three evaluated design provisions with regards to the computation of the sagging flexural resistance, $M_y^{*,+}$, is not significant. Therefore, the detailed approach presented in Eurocode 8-Part 1 (CEN 2004a) for calculating the slab effective width is not justified. Instead, this approach should be replaced with a simpler one (e.g., ANSI/AISC 360-16 AISC 2016b).
- The sagging flexural resistance, $M_y^{*,+}$, of shallow composite steel beams ($h < 500$ mm) is at least 1.4 times larger than that of deep beams. This value may vary considerably depending on the corresponding degree of composite action. In low rise steel frame buildings and/or steel buildings with space steel MRFs in which the degree of composite action is at least 0.4, the strong-column/weak-beam ratio shall be based on a beam's sagging flexural resistance.
- The hogging flexural resistance, $M_y^{*,-}$, of a composite steel beam is, on average, 10% larger than the corresponding one of the bare steel beam. This is attributed to the slab longitudinal reinforcement and the metal deck. The hogging plastic flexural resistance of a composite steel beam is sensitive to the steel material overstrength. This is traced well based on the ANSI/AISC 341-16 (AISC 2016a) seismic provisions because expected material properties are employed depending on the corresponding steel material grade. It is recommended that the material overstrength factors developed within the OPUS program (Braconi et al. 2013) are adopted in future editions of Eurocode 8-Part 1.
- Shallow composite steel beams ($h \leq 500$ mm) under sagging bending have an equivalent flexural stiffness of at least 1.6 times the effective flexural stiffness of the bare steel beam. This value decreases by up to 20% for deep composite steel beams ($h > 500$ mm). As such, the Eurocode (CEN 2004a, b) stiffness formulation exhibits higher dispersion because its estimation is not based on partially composite steel beams. Hence, the approaches discussed in the AISC and Japanese provisions are recommended for calculating the effective beam stiffness under sagging bending.
- The pre-capping plastic rotation capacity of composite steel beams is, on average, 50% higher than that of bare steel beams under sagging moment. When the beam is under hogging bending, the observed differences between composite and bare steel beams diminish. The Eurocode 8-Part 3 (CEN 2005a) formulations overestimate the measured plastic rotation capacities of steel beams in all the examined cases. This is attributed to the fact that the Eurocode approach does not consider the influence of the geometric and material properties of a steel beam on its plastic rotation capacity.
- The post-capping plastic rotation of composite steel beams is less sensitive to the presence of the slab. This is attributed to the fact that in the post-peak response, the slab is typically cracked, thereby becoming less effective in delaying local buckling-induced softening under cyclic loading.
- Empirical expressions are developed to reliably compute the plastic rotation capacity of composite steel beams. These expressions can be directly used for the seismic assessment of new and existing steel MRF systems based on nonlinear static analysis within the framework of Eurocode 8-Part 3 (CEN 2005a) and ASCE/SEI 41-17 (ASCE 2017). These expressions effectively capture the dependencies of pre- and post-capping plastic rotation capacities of composite steel beams with respect to the beam's geometric and steel material properties.
- System-level tests suggest that the plastic rotation capacity of interior beam-to-column connections is at least 50% larger than that of exterior joints due to the slab continuity that is not properly traced in typical beam-to-column subassembly experiments. This deserves more attention in future studies and requires system-level physical testing.
- The panel zone shear yield resistance is nearly the same in the three design provisions that were evaluated. However, Eurocode 3-Part 1-8 (CEN 2005c) is conservative if doubler plates exist on both sides of the column web. The reason is that one of the two doubler plates is disregarded from the computation of the panel zone shear resistance.
- The panel zone in wide-flange steel columns may be designed such that the relative panel zone-to-beam shear resistance, $V_{PZ,d} / V_{pl,b} = 0.8$. This value is based on composite steel beam test data for which at least a 5% peak story

drift ratio was attained. In these tests, the panel zones developed a total shear distortion up to about $10\gamma_y$ without experiencing pre-mature fracture within the corresponding beam-to-column connection.

6. Acknowledgments

This study is based on work supported by the Swiss National Science Foundation (Project No. 200021_169248). The financial support is gratefully acknowledged. Any opinions expressed in the paper are those of the authors and do not necessarily reflect the views of sponsors. The authors would like to sincerely thank Prof. Masayoshi Nakashima, Prof. Tomohiro Matsumiya, Prof. Roberto Leon, Prof. Gregory G. Deierlein, Prof. Gilberto Mosqueda, Dr. Paul Cordova, and Dr. Maikol Del Carpio for providing test data for the development of the composite steel beams database.

7. References

AIJ (2010a) Recommendation for limit state design of steel structures, 3rd edition. Architectural Institute of Japan

AIJ (2010b) Design recommendations for composite construction, 2nd edition. Architectural Institute of Japan

AISC (2016a) Seismic provisions for structural steel buildings, ANSI/AISC 341-16. American Institute for Steel Construction, Chicago, IL

AISC (2016b) Specification for structural steel buildings, ANSI/AISC 360-16. American Institute for Steel Construction, Chicago, IL

AISC (2016c) Prequalified connections for special and intermediate steel moment frames for seismic applications, ANSI/AISC 358-16. American Institute for Steel Construction, Chicago, IL

Araújo M, Macedo L, Castro JM (2017) Evaluation of the rotation capacity limits of steel members defined in EC8-3. J Constructional Steel Research 135:11–29. doi: 10.1016/j.jcsr.2017.04.004

Asada H, Matoba H, Tanaka T, Yamada S (2015) Retrofit effects for composite beams - Study on seismic retrofit of beam-to-column connection using supplemental H-section haunches Part 2. J Struct Constr Eng AIJ 80:1479–1487

ASCE (2017) Seismic evaluation and retrofit of existing buildings: ASCE standard ASCE/SEI 41-17. American Society of Civil Engineers, Reston, VA

Braconi A, Finetto M, Degee H, et al (2013) Optimising the seismic performance of steel and steel-concrete structures by standardising material quality control (OPUS). European Commission, Luxembourg

Bursi O, Haller M, Lennon T, et al (2009) Prefabricated composite beam-to-column filled tube or partially reinforced-concrete-encased column connections for severe seismic and fire loadings. European Commission, Luxembourg

Bursi OS, Gramola G (2000) Behaviour of composite substructures with full and partial shear connection under quasi-static cyclic and pseudo-dynamic displacements. Mater Struct 33:154–163. doi: 10.1007/BF02479409

Castro JM, Dávila-Arbona FJ, Elghazouli AY (2008) Seismic design approaches for panel zones in steel moment frames. J Earthq Eng 12:34–51. doi: 10.1080/13632460801922712

Castro JM, Elghazouli AY, Izzuddin BA (2007) Assessment of effective slab widths in composite beams. J Constr Steel Res 63:1317–1327. doi: 10.1016/j.jcsr.2006.11.018

CEN (2004a) EN 1998-1: Eurocode 8: Design of structures for earthquake resistance – Part 1: General rules, seismic actions and rules for buildings. European Committee for Standardization, Brussels, Belgium

CEN (2005a) EN 1998-3: Eurocode 8: Design of structures for earthquake resistance – Part 3: Assessment and retrofitting of buildings. European Committee for Standardization, Brussels, Belgium

CEN (2005b) EN 1993-1-1: Eurocode 3: Design of steel structures – Part 1-1: General rules and rules for buildings. European Committee for Standardization, Brussels, Belgium

CEN (2005c) EN 1993-1-8: Eurocode 3: Design of steel structures – Part 1-8: Design of joints. European Committee for Standardization, Brussels, Belgium

CEN (2004b) EN 1994-1-1: Eurocode 4: Design of composite steel and concrete structures – Part 1-1: General rules and rules for buildings. European Committee for Standardization, Brussels, Belgium

Chatterjee S, Hadi AS (2015) Regression analysis by example, 5th edition. John Wiley & Sons

Chen S-J, Chao YC (2001) Effect of composite action on seismic performance of steel moment connections with reduced beam sections. J Constr Steel Res 57:417–434. doi: 10.1016/S0143-974X(00)00022-5

Cheng C-T, Chan C-F, Chung L-L (2007) Seismic behavior of steel beams and CFT column moment-resisting connections with floor slabs. J Constr Steel Res 63:1479–1493. doi: 10.1016/j.jcsr.2007.01.014

Cheng C-T, Chen C-C (2005) Seismic behavior of steel beam and reinforced concrete column connections. J Constr Steel Res 61:587–606. doi: 10.1016/j.jcsr.2004.09.003

Ciutina AL, Dubina D (2003) Influence of column web stiffening on the seismic behaviour of beam-to-column joints. In: Proceedings of Stessa. pp 269–75

Civjan S, Engelhardt M, Gross J (2001) Slab effects in SMRF retrofit connection tests. J Struct Eng 127:230–237. doi: 10.1061/(ASCE)0733-9445(2001)127:3(230)

Cordova PP, Deierlein G (2005) Validation of the seismic performance of composite RCS frames: Full-scale testing, analytical modeling, and seismic design. The John A. Blume Earthquake Engineering Center, Stanford University, Stanford, CA

Del Carpio M, Mosqueda G, Lignos D (2014) Hybrid simulation of the seismic response of a steel moment frame building structure through collapse. Multidisciplinary Center for Earthquake Engineering Research, University at Bufalo

Du Plessis DP, Daniels JH (1972) Strength of composite beam-to-column connections. Fritz Engineering Laboratory, Lehigh University, Bethlehem, PA

Elkady A, Lignos DG (2014) Modeling of the composite action in fully restrained beam-to-column connections: implications in the seismic design and collapse capacity of steel special moment frames. Earthquake Eng. and Structural Dynamics 43:1935–1954. doi: 10.1002/eqe.2430

Elkady A, Lignos DG (2015) Effect of gravity framing on the overstrength and collapse capacity of steel frame buildings with perimeter special moment frames. Earthquake Eng. and Structural Dynamics 44:1289–1307. doi: 10.1002/eqe.2519

Engelhardt M, Venti M, Fry G, et al (2000) Behavior and design of radius-cut reduced beam section connections. SAC Joint Venture

Fardis MN (2018) Capacity Design: Early History. Earthquake Eng. and Structural Dynamics. doi: 10.1002/eqe.3110

Fujisawa K, Ichinohe Y, Sugimoto M, Sonoda M (2013) Statistical study on mechanical properties and chemical compositions of SN Steels. In: Summary of Technical Papers of Annual Meeting. Architectural Institute of Japan, pp 699–700

Hartloper A, Lignos D (2017) Updates to the ASCE 41-13 Provisions for the Nonlinear Modeling of Steel Wide Flange Columns for performance-basedearthquake engineering. In: The 8th European Conference on Steel and Composite Structures. Copenhagen, Denmark

Hirofumi A, Masayuki M (1985) Statistical investigation on mechanical properties of structural steel based on coupon tests. J Struct Constr Eng AIJ 94–105

Jones SL, Fry GT, Engelhardt MD (2002) Experimental evaluation of cyclically loaded reduced beam section moment connections. J Struct Eng 128:441–451. doi: 10.1061/(ASCE)0733-9445(2002)128:4(441)

Kanno R (2016) Advances in steel materials for innovative and elegant steel structures in Japan—A Review. Struct Eng Int 26:242–253. doi: 10.2749/101686616X14555428759361

Kim KD, Engelhardt MD (2002) Monotonic and cyclic loading models for panel zones in steel moment frames. J Constr Steel Res 58:605–635. doi: 10.1016/S0143-974X(01)00079-7

Kim S-Y, Lee C-H (2017) Seismic retrofit of welded steel moment connections with highly composite floor slabs. J Constr Steel Res 139:62–68. doi: 10.1016/j.jcsr.2017.09.010

Kim Y-J, Oh S-H, Moon T-S (2004) Seismic behavior and retrofit of steel moment connections considering slab effects. Eng Struct 26:1993–2005. doi: 10.1016/j.engstruct.2004.07.017

Kishiki S, Kadono D, Satsukawa K, Yamada S (2010) Consideration of composite effects on elasto-plastic behavior of panel zone. J Struct Constr Eng AIJ 75:1527–1536

Krawinkler H (1978) Shear in beam-column joints in seismic design of steel frames. Eng J 15:82-91

Krawinkler H (2009) Loading histories for cyclic tests in support of performance assessment of structural components. In: The 3rd International Conference on Advances in Experimental Structural Engineering. San Francisco

Lee C-H, Jeon S-W, Kim J-H, Uang C-M (2005) Effects of panel zone strength and beam web connection method on seismic performance of reduced beam section steel moment connections. J Struct Eng 131:1854–1865. doi: 10.1061/(ASCE)0733-9445(2005)131:12(1854)

Lee CH, Jung JH, Kim SY, Kim JJ (2016) Investigation of composite slab effect on seismic performance of steel moment connections. J Constr Steel Res 117:91–100. doi: 10.1016/j.jcsr.2015.10.004

Leon R (1990) Serviceability of composite floors. In: Proceedings of the 1990 National Steel Construction Conference. AISC, p 18

Leon R, Alsamsam I (1993) Performance and serviceability of composite floors. In: Structural Engineering in Natural Hazards Mitigation. ASCE, pp 1479–1484

Leon RT, Hajjar JF, Gustafson MA (1998) Seismic response of composite moment-resisting connections. I: Performance. J Struct Eng.124:868–876. doi: 10.1061/(ASCE)0733-9445(1998)124:8(868)

Lignos DG, Hikino T, Matsuoka Y, Nakashima M (2013) Collapse assessment of steel moment frames based on E-Defense full-scale shake table collapse tests. J Struct Eng.139:120–132. doi: 10.1061/(ASCE)ST.1943-541X.0000608

Lignos DG, Krawinkler H (2011) Deterioration modeling of steel components in support of collapse prediction of Steel moment frames under earthquake loading. J Struct Eng. 137:1291–1302. doi: 10.1061/(ASCE)ST.1943-541X.0000376

Lignos DG, Krawinkler H (2013) Development and utilization of structural component databases for performance-based earthquake engineering. J Struct Eng.139:1382–1394. doi: 10.1061/(ASCE)ST.1943-541X.0000646

Lu L, Xu Y, Zheng H (2017) Investigation of composite action on seismic performance of weak-axis column bending connections. J Constr Steel Res 129:286–300. doi: 10.1016/j.jcsr.2016.11.019

Mele E (2002) Moment resisting welded connections: an extensive review of design practice and experimental research in USA, Japan and Europe. J Earthquake Engineering 06:111–145. doi: 10.1142/S1363246902000590

Nakashima M, Matsumiya T, Suita K, Liu D (2005) Test on full-scale three-storey steel moment frame and assessment of ability of numerical simulation to trace cyclic inelastic behaviour. Earthquake Eng. and Structural Dynamics 35:3–19. doi: 10.1002/eqe.528

Nakashima M, Matsumiya T, Suita K, Zhou F (2007) Full-Scale test of composite frame under large cyclic loading. J Struct Engineering 133:297–304. doi: 10.1061/(ASCE)0733-9445(2007)133:2(297)

Nakashima M, Roeder C, Maruoka Y (2000) Steel moment frames for earthquakes in United States and Japan. J Structural Engineering 126:861–868. doi: 10.1061/(ASCE)0733-9445(2000)126:8(861)

Nam T, Kasai K (2012) Study on shake table experimental results regarding composite action of a full-scale steel building tested to collapse. In: 9th Int. Conference on Urban Earthquake Eng./4th Asia Conference on Earthquake Engineering. Tokyo Institute of Technology, Tokyo, pp 1111–1116

Panagiotakos TB, Fardis MN (2001) Deformations of reinforced concrete members at yielding and ultimate. Struct J 98:135–148

PEER/ATC (2010) Modeling and acceptance criteria for seismic design and analysis of tall buildings. Applied Technology Council (ATC), Redwood City, CA

Ricles JM, Fisher JW, Lu L-W, Kaufmann EJ (2002) Development of improved welded moment connections for earthquake-resistant design. J Constr Steel Res 58:565–604. doi: 10.1016/S0143-974X(01)00095-5

Roeder CW (2000) State of the art report on connection performance. Federal Emergency Management Agency, Washington D.C.

Roeder CW (2002) General issues influencing connection performance. J Structural Engineering 128:420–428. doi: 10.1061/(ASCE)0733-9445(2002)128:4(420)

Shin, S., Engelhardt, M. D. (2013). Cyclic Performance of Deep Column Moment Frames with Weak Panel Zones. In: Advances in Structural Engineering and Mechanics (ASEM13), Jeju, Korea.

Suita K, Yamada S, Tada M, et al (2008) Collapse experiment on four-story steel moment frame: Part 2. In: The 14th World Conference on Earthquake Engineering. Beijing

Sumner EA, Murray TM (2002) Behavior of extended end-plate moment connections subject to cyclic loading. J Struct Eng 128:501–508. doi: 10.1061/(ASCE)0733-9445(2002)128:4(501)

Tagawa Y, Kato B, Aoki H (1989) Behavior of composite beams in steel frame under hysteretic loading. J Struct Eng 115:2029–2045. doi: 10.1061/(ASCE)0733-9445(1989)115:8(2029)

Tremblay R, Tchebotarev N, Filiatrault A (1997) Seismic performance of RBS connections for steel moment resisting frames: Influence of loading rate and floor slab. In: Proceedings of Stessa

Uang C-M, Yu Q-S, Noel S, Gross J (2000) Cyclic testing of steel moment connections rehabilitated with RBS or welded haunch. J Structure Engineering 126:57–68. doi: 10.1061/(ASCE)0733-9445(2000)126:1(57)

Yamada S, Satsukawa K, Kishiki S, et al (2009) Elasto-plastic behavior of panel zone in beam to external column connection with concrete slab. J Struct Constr Eng AIJ 74:1841–1849

Zhang X, Ricles J, Lu L-W, Fisher J (2004) Development of seismic guidelines for deep-column steel moment connections. Lehigh University